

Article

Spin Cross-Over (SCO) Complex Based on Unsymmetrical Functionalized Triazacyclononane Ligand: Structural Characterization and Magnetic Properties

Merzouk Halit ^{1,2}, Mélissa Roger ¹, Véronique Patinec ¹, Said Yefsah ², Carlos J. Gómez-García ³  and Smail Triki ^{1,*} 

¹ University of Western Brittany, CNRS, CEMCA, 6 Avenue Le Gorgeu, C.S. 93837-29238 Brest Cedex 3, France; halitmerzouk@yahoo.fr (M.H.); roger.melissa@outlook.fr (M.R.); Veronique.Patinec@univ-brest.fr (V.P.)

² Faculté des Sciences, Université Mouloud Mammeri de Tizi-Ouzou (UMTO), 15000 Tizi Ouzou, Algeria; s.yefsah@yahoo.fr

³ Instituto de Ciencia Molecular (ICMol), Departamento de Química Inorgánica, Universidad de Valencia, C/Catedrático José Beltrán 2, 46980 Paterna, Spain; carlos.gomez@uv.es

* Correspondence: Smail.Triki@univ-brest.fr

Received: 21 December 2018; Accepted: 25 February 2019; Published: 7 March 2019



Abstract: The unsymmetrical ligand 1-(2-aminophenyl)-4,7-bis(pyridin-2-ylmethyl)-1,4,7-triazacyclononane (L6) has been prepared and characterized by NMR spectroscopy. The L6 ligand is based on the triazamacrocycle (tacn) ring that is functionalized by two flexible 2-pyridylmethyl and one rigid 2-aminophenyl groups. Reaction of this ligand with $\text{Fe}(\text{ClO}_4)_2 \cdot x\text{H}_2\text{O}$ led to the complex $[\text{Fe}(\text{L}6)](\text{ClO}_4)_2$ (**1**), which was characterized as the first Fe(II) complex based on the unsymmetrical N-functionalized tacn ligand. The crystal structure revealed a discrete monomeric $[\text{FeL}6]^{2+}$ entity in which the unsymmetrical N-functionalized triazacyclononane molecule (L6) acts as hexadentate ligand. As observed in the few parent examples that are based on the symmetrical N-functionalized tacn ligands, the triazacyclononane ring is facially coordinated and the N-donor atoms of the three functional groups (two pyridine and one aniline groups) are disposed in the same side of the tacn ring, leading to a distorted FeN_6 environment. The magnetic studies of **1** revealed the presence of an incomplete spin crossover (SCO) transition above 425 K, whose progress would be prevented by a very exothermic thermal decomposition at *ca.* 472 K, as shown by thermogravimetric and DSC measurements.

Keywords: Macrocycle ligands; Iron complex; High spin and Low spin; Spin Cross-Over; Magnetic properties

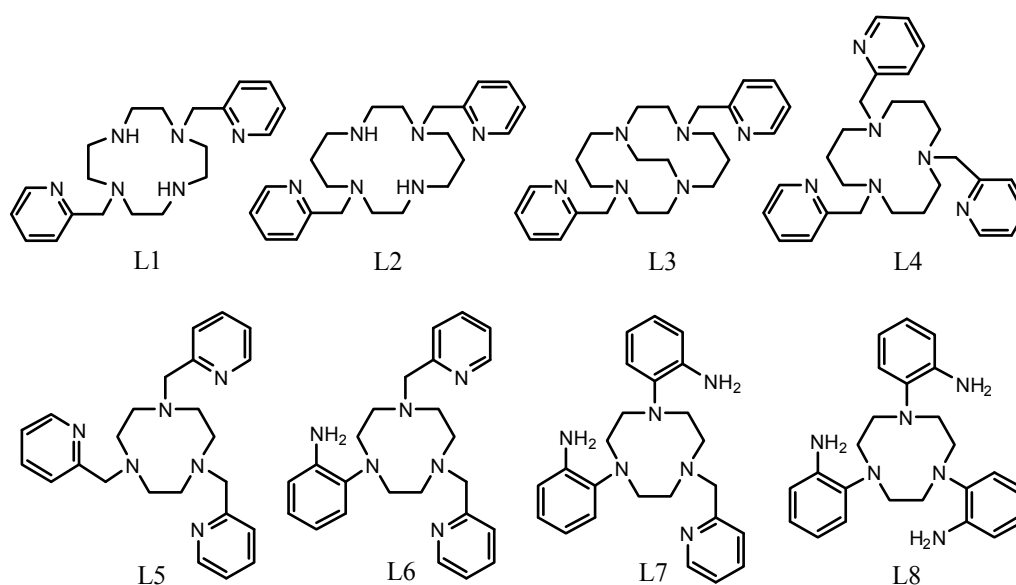
1. Introduction

Among the molecular switchable materials, the spin crossover (SCO) complexes are undoubtedly the most studied ones during the last decade, because of their several potential applications, including memory display devices [1–21]. Such complexes exhibit a reversible switch from the High Spin (HS) to the Low Spin (LS) state, as a response to an external perturbation as temperature, pressure, magnetic field, or light irradiation, when the complex involves metal ions having d^4 – d^7 electronic configuration [1–12]. To date, among the large number of SCO materials, the Fe(II) systems (d^6 configuration), for which the transition occurs between the paramagnetic high-spin (HS, $S = 2$, $^5T_{2g}$) and the diamagnetic low-spin (LS, $S = 0$, $^1A_{1g}$) states, are, by far, the most studied examples [13–21]. From the design point of view, a recent strategy consists in preparing SCO systems with the use of

polydentate ligands with a large potential denticity, such as cyclam and cyclen, which are known to form very stable complexes with transition metal ions [22]. However, even their remarkable reactivity toward transition metal ions, the limited number of the appropriate donor atoms that are involved in their corresponding macrocycle units, disallows some polydentate coordination modes, such as pentadentate or hexadentate coordination [22–32].

To increase their denticity and improve their coordination ability, several N-functionalization strategies of the tetraazamacrocycle molecules, such as cyclen and cyclam, have been studied using a number of synthetic routes for the mono-, di-, tri-, and tetra-N-alkylation [33–40]. This large synthetic work led to several series of stable metal complexes, in which the functionalized macrocycle molecule acts as penta-, hexa-, hepta-, or octa-dentate ligand [41–62]. Such metal complexes contribute to better understand the metal environment in some metalloenzymes and metalloproteins [63–66], better adapt chelators design to radiometals for radiopharmaceuticals [67,68], and also display catalytic properties [69] and, as reported in the last few years, original cooperative magnetic switching behaviors [41–43,50–52].

In this context, some of us have described two new systems of iron(II) monomeric complexes that are based on hexadentate functionalized tetraazamacrocycle ligands containing two 2-pyridylmethyl pendant arms, namely 1,7-bis(2'-pyridylmethyl)-1,4,7,10-tetraazacyclododecane (L1 in Scheme 1) and 1,8-bis(2'-pyridylmethyl)-1,4,8,11-tetraazacyclotetradecane (L2 in Scheme 1) [41,42]: the first one, $[\text{Fe}(\text{L1})](\text{BF}_4)_2$, containing the functionalized cyclen ligand (L1), remains in the high spin state ($S = 2$) in the whole temperature range, while the second one, $[\text{Fe}(\text{L2})](\text{BF}_4)_2 \cdot \text{H}_2\text{O}$, based on a slightly larger macrocycle (cyclam) presents a SCO transition with a transition temperature of *ca.* 150 K [41]. More recently, using the $[\text{Fe}^{\text{II}}\text{L2}]^{2+}$ cationic unit with different counter-anions ($(\text{C}(\text{CN})_3)^-$, $[\text{Ni}(\text{CN})_4]^{2-}$), we have shown that the SCO characteristics, such as the cooperativity and transition temperatures, can be fine-tuned by the nature of the counter-anion and by the co-crystallized water molecules [42]. One year later, B. Drahoš et al. [43], have enriched these SCO systems based on hexadentate macrocycle ligands with another series based on cross-bridged cyclam containing two 2-pyridylmethyl pendant arms (L3 in Scheme 1), for which they clearly discussed the crucial effect of the counter-anions and of the co-crystallized solvent molecules on the switching properties [43].



Scheme 1. Examples of hexadentate, tetra- and tri-azamacrocycle ligands involving three pyridylmethyl and/or aniline pendant arms.

In order to further investigate the effect of the size of the macrocycle ring of such hexadentate ligands on the coordination properties and ligand field, several Fe(II) systems that are based

on triazamacrocycle units involving pyridylmethyl, aniline, methylimidazol, methylpyrazol or methylthiophene groups have been reported [50–59]. However, to the best of our knowledge, only two systems have been described as SCO systems in the solid state [50,51]. Hendrickson et al. [50] reported the first series of Fe(II) complexes that are based on triazamacrocycles with three pyridylmethyl groups (L4 and L5 in Scheme 1): in the case of the nine-membered ring system (L5), the Fe(II) complex is LS, while the Fe(II) complex with larger 12-membered ring system (L4) exhibits a slight thermal dependence of the magnetic moment, suggesting a decrease of the ligand field energy with the increase of the macrocycle size. More recently, H. J. Shepherd et al. [51] have described an original detailed study on Fe(II) complex based on the nine-membered ring involving three aniline groups (L8 in Scheme 1), for which both magnetic and variable temperature single-crystal characterisations reveal a gradual SCO behaviour with a transition temperature of 281 K.

In view of the above observations, even if only based on two reports, such functionalized triazamacrocycle ligands appear as interesting ligands to design SCO materials with transition temperatures around or above room temperature, and more examples are needed not only to establish correlations between the magnetic coupling and the structural parameters, but also to obtain more structural data on structural features of both HS and LS states, which are essential in shedding light on the effect of the nature of the functional groups and/or the unsymmetrical character of the functionalized ligand on the SCO characteristics. In this context, we have designed a series of unsymmetrical N-functionalized triazacyclononane involving two different groups, such as the examples depicted in Scheme 1 (L6 and L7). In the present work, we report the synthesis of 1-(2-aminophenyl)-4,7-bis(pyridin-2-ylmethyl)-1,4,7-triazacyclononane (L6 in Scheme 1), as well as that of the corresponding Fe(II) complex $[\text{FeL6}](\text{ClO}_4)_2$ (**1**). We also report their spectroscopic and structural characterizations and the magnetic properties of the iron (II) complex **1**.

2. Results and Discussion

2.1. Synthesis

1,4-bis(pyridin-2-ylmethyl)-1,4,7-triazacyclononane (**A**) was synthesized, starting from the triazamacrocycle ligand (tacn) following the known orthoamide route that is already used for producing unsymmetrical N-functionalized tacn [55,61,62]. Reaction of **A** with one equivalent of 1-fluoro-2-nitrobenzene in distilled acetonitrile gave rise to an aromatic substitution between the secondary amine function and the aromatic ring that produced 1-(nitrophenyl)-4,7-bis(pyridin-2-ylmethyl)-1,4,7-triazacyclononane (**B**) as a bright orange compound in 50% yield (see Figures S1 and S2). The reduction of the nitro function into an amine function was carried out with hydrazine hydrate in ethanol with activated carbon. Ligand L6 was then obtained as a brown oil with a yield of 80% (See Figures S3 and S4). Single crystals of $[\text{FeL6}](\text{ClO}_4)_2$ (**1**) were obtained by slow evaporation of an aqueous solution containing the triazamacrocyclic ligand (L6) and $\text{Fe}(\text{ClO}_4)_2 \cdot x\text{H}_2\text{O}$ in a 1:1 ratio (See Figure S5).

2.2. Description of the Structure

The crystal structure of $[\text{Fe}(\text{L6})](\text{ClO}_4)_2$ (**1**) was determined at 150 K. The unit cell parameters, crystal and refinement data and pertinent bond distances and angles are summarized in Tables 1 and 2, respectively. The asymmetric unit of **1** is built from one Fe(II) ion (Fe), one 1-(2-aminophenyl)-4,7-bis(pyridin-2-ylmethyl)-1,4,7-triazacyclononane (L6) molecule, and two perchlorate anions, all being located on general positions (Figure 1 and Figure S6). The Fe(II) metal complex of **1** consists of a discrete monomeric $[\text{Fe}(\text{L6})]^{2+}$ cation in which the organic L6 ligand (Scheme 1) acts as hexadentate (Figure 1) whose two cationic charges are counterbalanced by two non-coordinated perchlorate anions.

The Fe(II) ion is hexa-coordinated by six N atoms: three of the macrocycle (N1, N2, and N3), two of the pyridine rings (N5 and N6), and one of the phenylamine ring (N4). Examination of the Fe-N bond distances and N-Fe-N bonds angles (see below) allows us to describe the metal environment

as a distorted FeN₆ octahedron, where the six Fe-N bond distances are quite similar, despite the different nature of the coordinated N atoms. Thus, the three Fe-N_{amine} bonds: Fe-N1 = 2.002(5) Å, Fe-N2 = 1.998(5) Å and Fe-N3 = 1.999(4) Å, the two Fe-N_{pyridine} bonds: Fe-N5 = 1.999(4) Å and Fe-N6 = 1.973(5) Å and the Fe-N_{phenylamine} bond: Fe-N4 = 2.005(5) Å are all very similar.

Table 1. Crystal data and structure refinement of compound [Fe(L6)](ClO₄)₂ (1).

1	
Formula	C ₂₄ H ₃₀ Cl ₂ FeN ₆ O ₈
F. Wt.	657.29
Space group	<i>P</i> 2 ₁ / <i>c</i>
Crystal system	Monoclinic
<i>a</i> /Å	9.3491(11)
<i>b</i> /Å	13.8911(17)
<i>c</i> /Å	20.308(2)
<i>α</i> /°	90
<i>β</i> /°	91.734(11)
<i>γ</i> /°	90
<i>V</i> /Å ³	2636.2(5)
<i>Z</i>	4
<i>T</i> /(K)	150
ρ_{calc} /g cm ⁻³	1.656
μ /mm ⁻¹	0.837
<i>F</i> (000)	1360
θ range (deg)	3.346–25.236
Total reflections	10476
Unique reflections	4754
R(int)	0.0899
Data with <i>I</i> > 2 σ (<i>I</i>)	2712
<i>N</i> _{var}	407
R ₁ ^a on <i>I</i> > 2 σ (<i>I</i>)	0.0698
<i>w</i> R ₂ ^b (all)	0.1613
GooF ^c on F ²	1.015
$\Delta\rho_{\text{max}}$ (eÅ ⁻³)	0.488
$\Delta\rho_{\text{min}}$ (eÅ ⁻³)	−0.495

^a R₁ = $\Sigma |F_o - F_c| / F_o$; ^b wR₂ = $[\Sigma((\omega(F_o^2 - F_c^2))^2 / (\omega F_o^2)^2)]^{1/2}$; ^c GooF = $[\Sigma(\omega(F_o^2 - F_c^2))^2 / (N_{\text{obs}} - N_{\text{var}})]^{1/2}$.

Table 2. Bond distances (Å) and angles (°) for compound [Fe(L6)](ClO₄)₂ (1).

Atoms	Distance	Atoms	Angle	Atoms	Angle	Atoms	Angle
Fe-N1	2.002(5)	N1-Fe-N2	86.4(2)	N2-Fe-N3	85.6(2)	N3-Fe-N5	168.2(2)
Fe-N2	1.998(5)	N1-Fe-N3	86.0(2)	N2-Fe-N4	170.00(19)	N3-Fe-N6	84.1(2)
Fe-N3	1.999(4)	N1-Fe-N4	84.2(2)	N2-Fe-N5	82.90(17)	N4-Fe-N5	94.66(17)
Fe-N4	2.005(5)	N1-Fe-N5	96.14(17)	N2-Fe-N6	98.58(19)	N4-Fe-N6	91.28(19)
Fe-N5	1.999(4)	N1-Fe-N6	168.49(17)	N3-Fe-N4	97.2(2)	N5-Fe-N6	94.76(17)
Fe-N6	1.973(5)						

The main distortion of the octahedral coordination around the Fe(II) atom is due to the bond angles (Table 2) that considerably deviate from the ideal values (the *cis* angles range from 82.9° to 98.6°, whereas the *trans* angles are in the range 168.2° to 170.0°). This high distortion is further confirmed by the relatively high values of the distortion parameter ($\Sigma = 63.0^\circ$) [70]. As observed in other similar tacn N-functionalized macrocycle ligands [50,51,57,71], the macrocycle is facially coordinated and the N-donor atoms of the three pendant groups (two pyridine and one aniline groups) are disposed in the same side of the macrocyclic ring, due to the small size of the triazamacrocyclic ring that forces the Fe(II) ion to be located over the flexible macrocycle. The distance of the Fe(II) metal ion to the plane defined by the three nitrogen atoms (N1, N2, and N3) is 1.232 Å. Careful examination of the

crystal packing in **1** reveals that the main intermolecular contacts are due the C-H \cdots O hydrogen bonds between the oxygen atoms of the perchlorate anions and the carbon atoms of the pyridine and aniline groups of the organic ligands (see Figure 2). The shortest C \cdots C contacts that were observed between adjacent tacn N-functionalized macrocycle ligands (C16 \cdots C23 = 3.655 Å and C4 \cdots C10 = 3.765 Å) are greater than twice the van der Waals radii (3.40 Å).

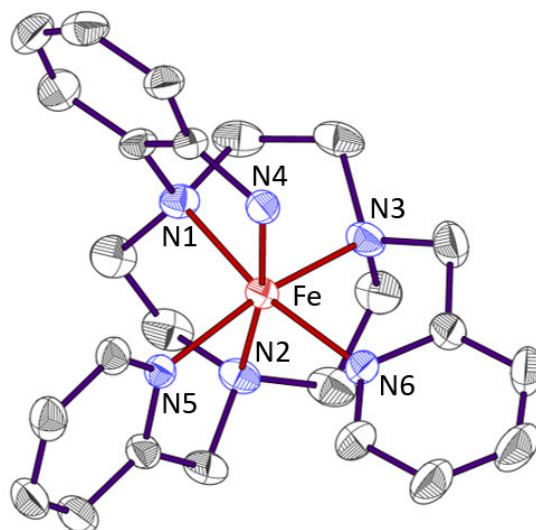


Figure 1. ORTEP [72] view of the cationic complex in $[\text{FeL6}](\text{ClO}_4)_2$ (**1**) showing thermal ellipsoids at 50% probability level, the atom labelling scheme and the coordination environment of the Fe(II) ion.

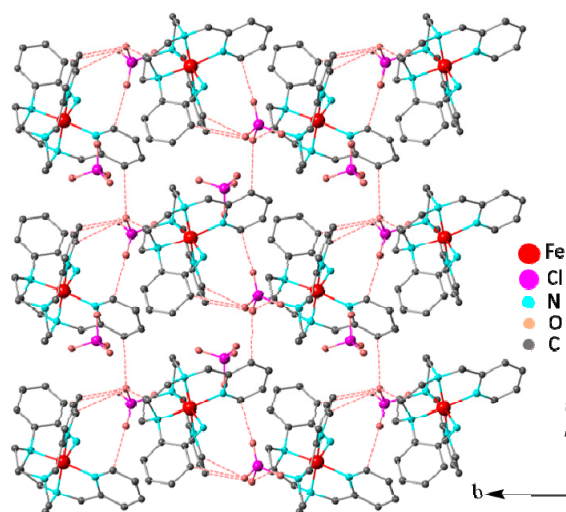


Figure 2. Shortest intermolecular contacts in the ab plane (C \cdots O distances in the range 2.95–3.22 Å).

2.3. Magnetic Properties

Variable temperature susceptibility measurements for **1** were carried out in the temperature range of 2–525 K. The thermal dependence of the product of the molar magnetic susceptibility times the temperature ($\chi_m T$) is depicted in Figure 3. The $\chi_m T$ product in the temperature range 20–300 K is constant and very low (*ca.* 0.09 cm³ K mol⁻¹), indicating that the Fe(II) centres are in the low spin (LS) configuration with a very small fraction of *ca.* 3% in the high spin (HS) configuration. On heating above 300 K, the $\chi_m T$ value shows a smooth and very tiny increase, reaching a value of *ca.* 0.2 cm³ K mol⁻¹ at 400 K. This initial increase suggests that the SCO initiate below 400 K, and consequently, the complete SCO transition would only be expected at higher temperatures ($T_{1/2} > 425$ K). However, in this high temperature region, the single crystal sample of **1** undergoes

decomposition at *ca.* 472 K (199 °C), as clearly revealed by thermogravimetric (TG) and differential scanning calorimetry (DSC) measurements that are detailed below (see also Figures S7 and S8), into HS iron(II) species, in agreement with the abrupt transition revealed at 480 K by the magnetic data (Figure 3). As expected, this sudden decomposition is irreversible and we could not measure any possible hysteresis, since the cooling scan shows a continuous increase of $\chi_m T$ when the temperature is decreased, suggesting the formation of iron(II) oxide upon decomposition.

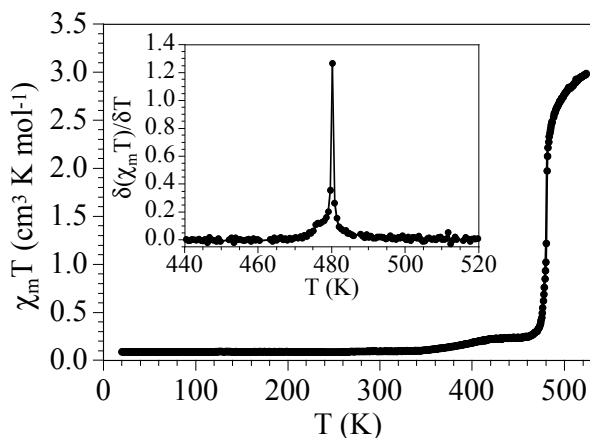


Figure 3. Thermal variation of the $\chi_m T$ product for complex **1**. Inset shows the thermal variation of the derivative of $\chi_m T$ as a function of temperature.

2.4. Thermogravimetric (TG) and Differential Scanning Calorimetry (DSC) Measurements

TG measurements of compound **1** (Figure S7) show a constant weight in the temperature range 298–450 K (25–177 °C) and a very smooth weight loss of less than 4% in the T range 450–472 K (177–199 °C), followed by a sudden decomposition accompanied by an explosion of the sample (that pushes down the crucible containing the sample resulting in a sudden weight increase to more than twice the initial weight, inset in Figure S7). This behavior suggests the presence of a very abrupt decomposition at *ca.* 472 K (199 °C).

The DSC measurements were performed in two different samples of compound **1** (Figure S8). The first sample shows an exothermic peak starting at *ca.* 450 K (177 °C) that ends at *ca.* 485 K (212 °C) when the heat that is produced in the exothermic decomposition exceeds the detection limit of our equipment without reaching a maximum. In order to check the possible reversibility of this abrupt exothermic transition, we measured a second sample in the same conditions with a heating/cooling cycle ending just before the abrupt transition (see experimental section). This cycle shows that, at 468 K (195 °C), the transition has already started and at this point it is still reversible, as shown by the second heating in sample 2, which perfectly matches the first heating scan.

Thus, TG and DSC experiments confirm the presence of a very abrupt irreversible exothermic transition at *ca.* 475 K (202 °C), with an explosion of the sample. Nevertheless, this transition is reversible if the heating is stopped before its completion.

2.5. Comparison with Other Related Complexes

In the following discussion, the average coordination distances $\langle \text{Fe-N} \rangle$ and the distortion parameter (Σ) will be used to assign the spin state on the Fe(II) crystallographic centers, since these parameters are known to be highly sensitive to the Fe(II) spin configuration (the typical $\langle \text{Fe-N} \rangle$ values are ~ 2.0 Å for the LS configuration and ~ 2.2 Å for the HS one and the Σ parameter is larger in the HS than in the LS configuration). Table 3 lists the Fe-N bond lengths and distortion parameters for [FeL6](ClO₄)₂ (**1**) and for two other Fe(II) complexes involving related N-functionalized triazacyclononane ligands ([FeL5](ClO₄)₂ (**2**) [50] and [FeL8](ClO₄)₂ (**3**) [51]. The average value of the six Fe-N distances for the three complexes (1.996(5) Å for **1** at 150 K, 1.990(6) Å for **2** at room

temperature and 2.020(2) Å for **3** at 120 K) are in good agreement with the values that are expected for the LS state of the Fe(II) ion in the FeN₆ distorted octahedral geometry, and they agree with the low magnetic moment (or close to zero) shown by the magnetic data for each complex (see Table 3).

Table 3. Fe-N distances (Å) and magnetic properties of the reported Fe(II) tacn N-functionalized macrocycle based complexes (see Scheme 1 for L5, L6, and L8).

Fe(II) Complex	[FeL6](ClO ₄) ₂ (1)	[FeL5](ClO ₄) ₂ (2)	[FeL8](ClO ₄) ₂ (3)
T (K)	150	298	120
Fe-N(tacn)	2.002(5)	2.001(6)	2.001(2)
	1.998(5)	2.001(6)	1.999(2)
	1.999(4)	2.001(6)	1.996(2)
Fe-N(py)	1.999(4)	1.979(6)	-
	1.973(5)	1.979(6)	-
	-	1.979(6)	-
Fe-N(aniline)	2.005(5)	-	2.053(2)
	-	-	2.037(2)
	-	-	2.035(2)
<d _(Fe-N) >	1.996(5)	1.990(6)	2.020(2)
^a Σ (°)	63(1)	64(1)	56(1)
Magnetic behavior	SCO T _{1/2} > 425 K	LS (T < 406 K) *	Gradual SCO T _{1/2} = 281 K
Reference	This work	50	51

^aΣ is the sum of the deviation from 90° of the 12 *cis*-angles of the FeN₆ octahedron [70]. * The magnetic properties have been performed in the temperature range 303–406 K in which the complex (**2**) is essentially LS.

In the LS state of the three complexes, the Fe-N(tacn) (1.998–2.002 Å for **1**, 2.001(6) Å for **2** and 1.996–2.001 Å for **3**) and the Fe-N(py) distances (Fe-N5 1.999(4) Å, Fe-N6 1.973(5) Å for **1** and 1.979(6) Å for **2**) associated to the tertiary amine and to the pyridine nitrogen atoms, respectively, are in the same range, while the corresponding distances that arise from the coordination of the aniline groups, Fe-N(aniline), associated to the primary amine, are significantly longer (Fe-N4 2.005(5) Å for **1**; 2.053(2), 2.037(2) and 2.035(2) Å for **3**). This difference may be attributed to the more rigid aniline group for which the steric constraints should prevent strong Fe-N bonds. The distortion parameters that are depicted in Table 3 indicate that the FeN₆ environments are highly distorted for the three complexes, even in the LS state. These parameters also indicate a less distorted environment for complex **3**, which may be at the origin of the lower transition temperature that was observed for this compound.

3. Experimental Section

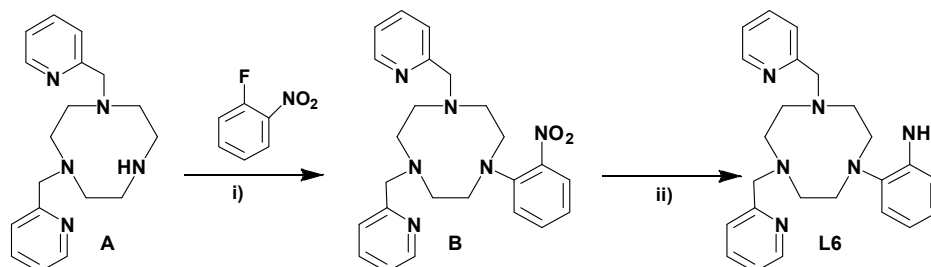
3.1. Starting Materials

Solvents and reagents were obtained from commercial suppliers and they were used without further purification. 1,4,7-Triazacyclononane (tacn) was purchased from CheMatech (Dijon, France).

3.2. Synthesis of 1-(2-Nitrophenyl)-4,7-bis(pyridin-2-ylmethyl)-1,4,7-triazacyclononane (**B**)

1-fluoro-2-nitrobenzene (170 µL, 1.6 mmol) was slowly added to a solution of 1,4-bis(pyridin-2-ylmethyl)-1,4,7-triazacyclononane (**A**) (450 mg, 1.4 mmol) in distilled acetonitrile (20 mL) with potassium carbonate (1.0 g, 7 mmol) (Scheme 2). The reaction mixture was stirred and refluxed under nitrogen atmosphere during two days. The hot solution was filtrated and the filtrate was evaporated under reduced pressure. The residue was purified by alumina chromatography (hexane/CH₂Cl₂: 8/2 then CH₂Cl₂) to yield an orange oil (350 mg, 0.8 mmol, 50%). ¹H NMR (CDCl₃, 300 MHz), 2.81 (4H, s, CH₂tacn), 3.03 (4H, m, CH₂tacn), 3.48 (4H, m, CH₂tacn), 3.86 (4H, s, CH₂), 6.79 (1H, t H_{Ph}), 7.02 (1H, d,

H_{Ph}), 7.12 (2H, m, H_{Pyr}), 7.34 (1H, t, H_{Ph}), 7.43 (2H, d, H_{Pyr}), 7.54–7.62 (3H, m, $H_{Ph} + H_{Pyr}$), and 8.48 (2H, d, H_{Pyr}). ^{13}C NMR ($CDCl_3$, 75.4 MHz) 53.9, 55.1, 55.6 (CH_{2tacn}), 63.8 (CH_2), 118.5 120.4 (CH_{Ph}), 122.1 123.4 (CH_{Pyr}), 126.0, 132.7 (CH_{Ph}), 136.4 144.2 (CH_{Pyr}), and 148.9 (C_{Ph}) (see Figures S1 and S2).



Scheme 2. Ligand synthesis: i) CH_3CN , K_2CO_3 , reflux, 48 h under N_2 ; and, ii) NH_2NH_2 , H_2O /Ethanol, activated carbon, three days under N_2 .

3.3. Synthesis of 1-(2-Aminophenyl)-4,7-bis(pyridin-2-ylmethyl)-1,4,7-triazacyclononane (L6)

1-(2-nitrophenyl)-4,7-bis(pyridin-2-ylmethyl)-1,4,7-triazacyclononane (**B**) (350 mg, 0.8 mmol) in 15 mL of absolute ethanol was stirred with an excess of hydrazine monohydrate (5 mL) with activated carbon under reflux under nitrogen atmosphere during three days (Scheme 2). The solution was filtrated and then evaporated under reduced pressure. The residue was dissolved in $CHCl_3$ (20 mL) and $MgSO_4$ was added. The solution was filtrated and the filtrate was evaporated under reduced pressure to yield a brown oil (260 mg, 80%). 1H NMR ($CDCl_3$, 300 MHz), 2.90 (4H, m, CH_{2tacn}), 2.98 (4H, m, CH_{2tacn}), 3.21 (4H, m, CH_{2tacn}), 3.88 (4H, m, CH_2), 6.66 (2H, m, H_{Ph}), 6.86 (1H, t, H_{Ph}), 7.02 (1H, d, H_{Ph}), 7.15 (2H, t, H_{Pyr}), 7.44 (2H, d, H_{Pyr}), 7.65 (2H, td, H_{Pyr}), 8.49 (2H, m, H_{Pyr}); ^{13}C NMR ($CDCl_3$, 75.4 MHz), 55.2, 56.3, 56.9 (CH_{2tacn}), 64.6 (CH_2), 115.1 117.6 (CH_{Ph}), 121.9 123.2 (CH_{Pyr}), 123.1 124.0 (CH_{Ph}), 136.2 (CH_{Pyr}), 140.0 143.0 (C_{Ph}), 149.0 (CH_{Pyr}), and 159.9 (C_{Pyr}) (see Figures S3 and S4).

3.4. Synthesis of $[Fe(L6)](ClO_4)_2$ (**1**)

Complex $[Fe(L6)](ClO_4)_2$ (**1**) was prepared, as single crystals, using the slow-diffusion procedure in a fine glass tube. A solution of L6 (2 mL, 18×10^{-3} M) in CH_2Cl_2/Et_2O :1/1 was placed in a capillary of 0.5 mm diameter. A solution of $Fe(ClO_4)_2 \cdot xH_2O$ (2 mL, 18×10^{-3} M) in methanol (2 mL) was slowly added. After three days, slow diffusion at room temperature gave red prismatic crystals of $[Fe(L6)](ClO_4)_2$ (**1**). Elemental analysis: % calculated for $C_{24}H_{30}Cl_2FeN_6O_8$ (**1**): C, 43.8; N, 12.8; H, 4.6. Found: C, 44.1; N, 13.0; H, 4.6. IR data (ν/cm^{-1}): 3307(w), 1613(w), 1481(m), 1451(m), 1340(w), 1292(w), 1162(w), 1065(s), 1001(br), 829(w), 803(m), 758(s), 722(w), 619(s), 573(w), 552(w), 501(m), and 436(w) (see supporting information, Figure S5).

3.5. Characterization of the Materials

Elemental analyses were performed by the “Service Central d’Analyses du CNRS”, Gif-sur-Yvette, France. Infrared spectra were recorded in the range 4000–200 cm^{-1} on a FT-IR BRUKER ATR VERTEX70 Spectrometer. Diffraction analyses were performed using an Oxford Diffraction Xcalibur κ -CCD diffractometer. Mass analyses were carried out by the “Service Central d’Analyses du CNRS”, Vernaison, France. NMR spectra were recorded on a Bruker AMX-3 300 (300 MHz).

3.6. Magnetic Measurements

Magnetic susceptibility measurements were carried out in the temperature range 2–525 K, with an applied magnetic field of 0.1 T on a polycrystalline sample of compound **1** with a Quantum Design MPMS-XL-5 SQUID susceptometer (San Diego, CA, USA). The susceptibility data were corrected for the sample holder that was previously measured using the same conditions and for the diamagnetic contributions of the salt, as deduced by using Pascal’s constant tables [48].

3.7. Thermogravimetric (TG) and Differential Scanning Calorimetry (DSC) Measurements

TG measurements were performed in Pt crucibles with a TA instruments TGA 550 thermobalance equipped with an autosampler. The measurements were done in the 30–700 °C temperature range at 10 °C/min under a N₂ flux of 60 mL/min. DSC measurements were performed in Aluminium crucibles with a TA instruments Q20 Differential Scanning Calorimeter in two different samples of compound **1**. Sample 1 was measured with a heating scan from 25 to 212 °C at 10 °C/min under a N₂ flux of 50 mL/min. Sample 2 was measured in the same conditions with the following protocol: (i) a first heating scan from 25 to 195 °C, (ii) a cooling scan from 195 to 25 °C and (iii) a second heating scan from 25 to 205 °C.

3.8. Crystallographic Data Collection and Refinement

The crystallographic study of **1** was performed at 150 K using an Oxford Diffraction Xcalibur-CCD diffractometer equipped with a graphite monochromated MoK α radiation ($\lambda = 0.71073 \text{ \AA}$). The full sphere data collections were performed using 1.0° ω -scans with an exposure time of 60 s per frame. Data collection and data reduction were done with the CRYALIS-CCD and CRYALIS-RED programs on the full set of data [73]. The crystal structures were solved by direct methods and successive Fourier difference syntheses and were refined on F^2 by weighted anisotropic full-matrix least-square methods [74]. All non-hydrogen atoms were anisotropically refined and the hydrogen atoms were calculated and included as isotropic fixed contributors to F_c . All other calculations were performed with standard procedures (OLEX2) [75]. Crystal data, structure refinement and collection parameters are listed in Table 1. Room-temperature X-ray powder diffraction spectrum (XRPD) was recorded on a PANalytical Empyrean X-ray powder diffractometer at 45 kV, 40 mA with a Cu-target tube. As clearly indicated by Figure S9, the measured pattern of microcrystalline powder of **1** is qualitatively similar to the pattern that was derived from the single-crystal crystallographic data.

CCDC-1880523 contains the supplementary crystallographic data for compound **1**. These data can be obtained free of charge from The Cambridge Crystallographic Data Centre at www.ccdc.cam.ac.uk/data_request/cif.

4. Conclusions

The new functionalized 1-(2-aminophenyl)-4,7-bis(pyridin-2-ylmethyl)-1,4,7-triazacyclononane (L6) was prepared from starting tacn, followed by the orthoamide route that is already used for producing unsymmetrical N-functionalized tacn [55,61,62] by an aromatic substitution using 1-fluoro-2-nitrobenzene and by a reduction of the nitro function into an amine function. Its corresponding Fe(II) complex, [Fe(L6)](ClO₄)₂ (**1**), has been prepared and structurally characterized as the first Fe(II) complex based on unsymmetrical N-functionalized tacn ligand. As the parent complexes involving symmetrical N-functionalized tacn ligands (L5 and L8, in Scheme 1) [50,51], the [Fe(L6)]²⁺ complex displays a discrete structure in which the macrocycle ring is facially coordinated and the N-donor atoms arise from the three functional groups (two pyridine and one aniline groups), are located on the same side of the tacn macrocyclic unit. The magnetic studies of **1** revealed the presence of an incomplete spin crossover (SCO) transition above 425 K, whose progress would be prevented by a very exothermic thermal decomposition at *ca.* 472 K, as shown by thermogravimetric and DSC measurements. Finally, the symmetrical and unsymmetrical characters of the substituted tacn ligands (L6) in **1** do not play an important role in the value of the transition temperatures, since complex **3**, which involves symmetrical ligand (L8), exhibits SCO transition at a lower temperature (281 K) compared to complexes **1–2**, involving unsymmetrical (L6) and symmetrical (L5) ligands, respectively. Thus, the lower transition temperature observed for complex **3** should be associated to the coordination of six σ -donor nitrogen atoms (3 sp^3 N atoms from the tacn cycle and 3 sp^3 N atoms from the aniline groups), which should favour the presence of lower crystal field energy than in complexes **1** and **2** involving two and three pyridine groups with π -acceptor character, respectively.

Supplementary Materials: The following are available online at <http://www.mdpi.com/2312-7481/5/1/19/s1>, Figure S1: ^1H NMR spectrum of compound **B** (CDCl_3 , 300 MHz, 25 °C), Figure S2: ^{13}C NMR spectrum of compound **B** (CDCl_3 , 75.4 MHz, 25 °C), Figure S3: ^1H NMR spectrum of compound **L6** (CDCl_3 , 300 MHz, 25 °C), Figure S4: ^{13}C NMR spectrum of compound **L6** (CDCl_3 , 75.4 MHz, 25 °C), Figure S5: IR data (ν/cm^{-1}) spectrum of complex $[\text{Fe}(\text{L6})](\text{ClO}_4)_2$ (**1**), Figure S6: Structure of cationic complex of **1** showing the atom labelling scheme and the coordination environment of the Fe(II) ion, Figure S7: Thermogravimetric measurements of compound **1** at a heating rate of 10 K/min in the temperature range 300–980 K. Inset shows a zoom of the decomposition peak at ca. 472 K, Figure S8: DSC scans for two different samples of compound **1** for different heating and cooling scans at a scan rate of 10 K/min, Figure S9: Observed and calculated X-ray powder diffraction patterns for complex **1**, Table S1: Selected bond distances (Å) for complex **1** (see Figure S6 for the atom labelling scheme), Table S2: Selected bond angles (°) for complex **1** (see Figure S6 for the atom labelling scheme).

Author Contributions: M.H. and M.R. synthesized the ligand, the metal complex and made the first experimental characterisations. V.P. supervised the organic syntheses and interpreted the NMR spectra. S.Y. analysed the crystal data of the metal complex at 150 K. C.J.G.-G. performed and interpreted the magnetic measurements, the TG and DSC measurements. S.T. supervised the experimental work and wrote the manuscript on which all the authors have contributed.

Funding: This research was funded by the French CNRS, the “Université de Brest”, the Région Bretagne (MR) and the “Agence Nationale de la Recherche” (ANR project BISTA-MAT: ANR-12-BS07-0030-01). Generalitat Valenciana (Prometeo project) and the Spanish MINECO (Project CTQ2017-87201-P AEI/FEDER, EU).

Acknowledgments: ST greatly thanks Prof. Philippe Guionneau from University of Bordeaux, ICMCB, UMR 5026, France, for having supplied the supplementary X-ray data concerning compound $[\text{FeL8}](\text{ClO}_4)_2$ (**3**).

Conflicts of Interest: The authors declare no conflict of interest.

References

1. Kumar, K.S.; Ruben, M. Emerging trends in spin crossover (SCO) based functional materials and devices. *Coord. Chem. Rev.* **2017**, *346*, 176–205. [[CrossRef](#)]
2. Shalabaeva, V.; Ridier, K.; Rat, S.; Manrique-Juarez, M.D.; Salmon, L.; Séguy, I.; Rotaru, A.; Molnár, G.; Bousseksou, A. Room temperature current modulation in large area electronic junctions of spin crossover thin films. *Appl. Phys. Lett.* **2018**, *112*, 013301. [[CrossRef](#)]
3. Dugay, J.; Giménez-Marqués, M.; Kozlova, T.; Zandbergen, H.W.; Coronado, E.; van der Zant, H.S.J. Spin Switching in Electronic Devices Based on 2D Assemblies of Spin-Crossover Nanoparticles. *Adv. Mater.* **2015**, *27*, 1288–1293. [[CrossRef](#)] [[PubMed](#)]
4. Jeon, I.-R.; Park, J.G.; Haney, C.R.; Harris, T.D. Spin crossover iron(II) complexes as PARACEST MRI thermometers. *Chem. Sci.* **2014**, *5*, 2461–2465. [[CrossRef](#)]
5. Baadji, N.; Sanvito, S. Giant Resistance Change across the Phase Transition in Spin-Crossover Molecules. *Phys. Rev. Lett.* **2012**, *108*, 217201. [[CrossRef](#)] [[PubMed](#)]
6. Prins, F.; Monrabal-Capilla, M.; Osorio, E.A.; Coronado, E.; van der Zant, H.S.J. Room-Temperature Electrical Addressing of a Bistable Spin-Crossover Molecular System. *Adv. Mater.* **2011**, *23*, 1545–1549. [[CrossRef](#)] [[PubMed](#)]
7. Bousseksou, A.; Negre, N.; Goiran, M.; Salmon, L.; Tuchagues, J.P.; Boillot, M.L.; Boukheddaden, K.; Varret, F. Dynamic triggering of a spin-transition by a pulsed magnetic field. *Eur. Phys. J. B* **2000**, *13*, 451–456.
8. Bousseksou, A.; Molnár, G.; Salmon, L.; Nicolazzi, W. Molecular spin crossover phenomenon: Recent achievements and prospects. *Chem. Soc. Rev.* **2011**, *40*, 3313–3335. [[CrossRef](#)] [[PubMed](#)]
9. Gütllich, P.; Goodwin, H.A. (Eds.) *Spin Crossover in Transition Metal Compounds*; Springer: Berlin/Heidelberg, Germany, 2004; Volume 233–235.
10. Linares, J.; Codjovi, E.; Garcia, Y. Pressure and Temperature Spin Crossover Sensors with Optical Detection. *Sensors* **2012**, *12*, 4479–4492. [[CrossRef](#)] [[PubMed](#)]
11. Gütllich, P.; Gaspar, A.B.; Garcia, Y. Spin state switching in iron coordination compounds. *Beilstein J. Org. Chem.* **2013**, *9*, 342–391. [[CrossRef](#)] [[PubMed](#)]
12. Jureschi, C.-M.; Linares, J.; Boulmaali, A.; Dahoo, P.R.; Rotaru, A.; Garcia, Y. Pressure and Temperature Sensors Using Two Spin Crossover Materials. *Sensors* **2016**, *16*, 187. [[CrossRef](#)] [[PubMed](#)]

13. Halcrow, M.A. (Ed.) *Spin-Crossover Materials, Properties and Applications*; John Wiley & Sons Ltd.: Oxford, UK, 2013.
14. Mekuimemba, A.D.; Conan, F.; Mota, A.-J.; Palacios, M.-A.; Colacio, E.; Triki, S. On the Magnetic Coupling and Spin Crossover Behavior in Complexes Containing the Head-to-Tail $[\text{Fe}^{\text{II}}_2(\mu\text{-SCN})_2]$ Bridging Unit: A Magnetostructural Experimental and Theoretical Study. *Inorg. Chem.* **2018**, *57*, 2184–2192. [[CrossRef](#)] [[PubMed](#)]
15. Pittala, N.; Thétiot, F.; Triki, S.; Boukheddaden, K.; Chastanet, G.; Marchivie, M. Cooperative 1D Triazole-Based Spin Crossover Fe^{II} Material With Exceptional Mechanical Resilience. *Chem. Mater.* **2017**, *29*, 490–494. [[CrossRef](#)]
16. Phan, H.; Hrudka, J.J.; Igimbayeva, D.; Lawson Daku, L.M.; Shatruk, M. A Simple Approach for Predicting the Spin State of Homoleptic Fe(II) Tris-diimine Complexes. *J. Am. Chem. Soc.* **2017**, *139*, 6437–6447. [[CrossRef](#)] [[PubMed](#)]
17. Pittala, N.; Thétiot, F.; Charles, C.; Triki, S.; Boukheddaden, K.; Chastanet, G.; Marchivie, M. An unprecedented trinuclear Fe^{II} triazole-based complex exhibiting a concerted and complete sharp spin transition above room temperature. *Chem. Commun.* **2017**, *53*, 8356–8359. [[CrossRef](#)] [[PubMed](#)]
18. Milin, E.; Patinec, V.; Triki, S.; Bendeif, E.-E.; Pillet, S.; Marchivie, M.; Chastanet, G.; Boukheddaden, K. Elastic Frustration Triggering Photoinduced Hidden Hysteresis and Multistability in a Two-Dimensional Photoswitchable Hofmann-Like Spin-Crossover Metal–Organic Framework. *Inorg. Chem.* **2016**, *55*, 11652–11661. [[CrossRef](#)] [[PubMed](#)]
19. Shatruk, M.; Phan, H.; Chrisostomo, B.A.; Suleimenova, A. Symmetry-breaking structural phase transitions in spin crossover complexes. *Coord. Chem. Rev.* **2015**, *289–290*, 62–73. [[CrossRef](#)]
20. Atmani, A.; El Hajj, F.; Benmansour, S.; Marchivie, M.; Triki, S.; Conan, F.; Patinec, V.; Handel, H.; Dupouy, G.; Gómez-García, C.J. Guidelines to design new spin crossover materials. *Coord. Chem. Rev.* **2010**, *254*, 1559–1569. [[CrossRef](#)]
21. Coronado, E.; Galán-Mascarós, J.R.; Monrabal-Capilla, M.; García-Martínez, J.; Pardo-Ibáñez, P. Bistable Spin-Crossover Nanoparticles Showing Magnetic Thermal Hysteresis near Room Temperature. *Adv. Mater.* **2007**, *19*, 1359–1361. [[CrossRef](#)]
22. Bianchi, A.; Micheloni, M.; Paoletti, P. Thermodynamic aspects of the polyazacycloalkane complexes with cations and anions. *Coord. Chem. Rev.* **1991**, *110*, 17–113. [[CrossRef](#)]
23. Lord, R.L.; Schultz, F.A.; Baik, M.-H. Spin Crossover-Coupled Electron Transfer of $[\text{M}(\text{tacn})_2]^{3+/2+}$ Complexes (tacn = 1,4,7-Triazacyclononane; M = Cr, Mn, Fe, Co, Ni). *J. Am. Chem. Soc.* **2009**, *131*, 6189–6197. [[CrossRef](#)] [[PubMed](#)]
24. Krüger, H.-J. Spin transition in octahedral metal complexes containing tetraazamacrocyclic ligands. *Coord. Chem. Rev.* **2009**, *253*, 2450–2459. [[CrossRef](#)]
25. Long, N.J.; Parker, D.G.; Speyer, P.R.; White, A.J.P.; Williams, D.J. Synthesis, characterisation and polymerisation of vinylbenzene-substituted triazacyclododecanes and their transition metal complexes. *J. Chem. Soc. Dalton Trans.* **2002**, *10*, 2142–2150. [[CrossRef](#)]
26. Blakesly, A.W.; Payne, S.C.; Hagen, K.S. Spin-State Variation in Solid State and Solution of Mononuclear Iron(II) 1,4,7-Trimethyl-1,4,7-triazacyclonane Complexes. *Inorg. Chem.* **2000**, *39*, 1979–1989. [[CrossRef](#)]
27. Walf, A.H.; Benda, R.; Litterst, F.J.; Stebani, U.; Schmidt, S.; Lattermann, G. Liquid Crystalline Octahedral Iron(III) Complexes with 1,4,7-Tris[3,4-bis(decyloxy)benzyl]-1,4,7-triazacyclononane: Thermal Characterization and Mössbauer Investigations of Bridging and Redox Behavior. *Chem. Eur. J.* **1998**, *4*, 93–99. [[CrossRef](#)]
28. Fallis, I.A.; Griffiths, P.C.; Hibbs, D.E.; Hursthouse, M.B.; Winington, A.L. Solid state and solution behaviour of novel transition metal containing surfactants. *Chem. Commun.* **1998**, *6*, 665–666. [[CrossRef](#)]
29. Farrugia, L.J.; Lovatt, P.A.; Peacock, R.D. Synthesis of a series of novel binucleating ligands based on 1,4,7-triazacyclononane and o-, m- and p-xylene: Crystal structure of the μ -hydroxy-bridged dicopper(II) complex $[\text{Cu}_2\text{L}^m(\text{OH})_2][\text{BPh}_4]_2$ [$\text{L}^m = \alpha, \alpha'$ -bis (N-1,4,7-triazacyclononane)-m-xylene]. *J. Chem. Soc. Dalton Trans.* **1997**, *6*, 911–912. [[CrossRef](#)]
30. Turner, J.W.; Schultz, F.A. Solution Characterization of the Iron(II) Bis(1,4,7-Triazacyclononane) Spin-Equilibrium Reaction. *Inorg. Chem.* **2001**, *40*, 5296–5298. [[CrossRef](#)] [[PubMed](#)]
31. Dabrowiak, J.C.; Merrel, P.H.; Busch, D.H. High- and low-spin six-coordinate complexes of iron(II) with a saturated tetradentate macrocyclin ligand. *Inorg. Chem.* **1972**, *11*, 1979–1988. [[CrossRef](#)]

32. Goedken, V.L.; Merrell, P.H.; Busch, D.H. Complexes of Iron (II) and Iron (III) with the Tetradentate Macrocycle 5,7,7,12,14,14-Hexamethyl-1,4,8,11-tetraazacyclotetradeca-4,11-diene. *J. Am. Chem. Soc.* **1972**, *94*, 3397–3405. [[CrossRef](#)]
33. Lindoy, L.F. *The Chemistry of Macrocyclic Ligand Complexes*; Cambridge University Press: Cambridge, UK, 1989.
34. Parker, D. (Ed.) *Macrocycle Synthesis: A Practical Approach*; Oxford University Press: Oxford, UK, 1996.
35. Fensterbank, A.; Zhu, J.; Riou, D.; Larpent, C. A convenient one-step synthesis of mono-*N*-functionalized tetraazamacrocycles. *J. Chem. Soc. Perkin Trans.* **1999**, *1*, 811–816. [[CrossRef](#)]
36. Helps, A.M.; Parker, D.; Morphy, J.R.; Chapman, J. General routes for the synthesis of mono, di and tri-*N*-substituted derivatives of cyclam. *Tetrahedron* **1989**, *45*, 219–226. [[CrossRef](#)]
37. Royal, G.; Dahaoui-Gindrey, V.; Dahaoui, S.; Tabard, A.; Guilard, R.; Pullumbi, P.; Lecomte, C. New Synthesis of *trans*-Disubstituted Cyclam Macrocycles—Elucidation of the Disubstitution Mechanism on the Basis of X-ray Data and Molecular Modeling. *Eur. J. Org. Chem.* **1998**, *1998*, 1971–1975. [[CrossRef](#)]
38. Davies, P.J.; Taylor, M.R. Formation of 1,11-bis(pendant donor)-cyclam derivatives via the formamidinium salt (cyclam = 1,4,8,11-tetraazacyclotetradecane). *Chem. Commun.* **1998**, *7*, 827–828. [[CrossRef](#)]
39. Bellouard, F.; Chuburu, F.; Kervarec, N.; Toupet, L.; Triki, S.; Le Mest, Y.; Handel, H. *cis*-Diprotected cyclams and cyclens: A new route to symmetrically or asymmetrically 1,4-disubstituted tetraazamacrocycles and to asymmetrically tetrasubstituted derivatives. *J. Chem. Soc. Perkin Trans.* **1999**, *1*, 3499–3505. [[CrossRef](#)]
40. Mishra, A.K.; Draillard, K.; Faivre-Chauvet, A.; Gestin, J.-F.; Curtet, C.; Chatal, J.-F. A convenient, novel approach for the synthesis of polyaza macrocyclic bifunctional chelating agents. *Tetrahedron Lett.* **1996**, *37*, 7515–7518. [[CrossRef](#)]
41. El Hajj, F.; Sebki, G.; Patinec, V.; Marchivie, M.; Triki, S.; Handel, H.; Yefsah, S.; Tripier, R.; Gómez-García, C.J.; Coronado, E. Macrocycle-Based Spin-Crossover Materials. *Inorg. Chem.* **2009**, *48*, 10416–10423. [[CrossRef](#)] [[PubMed](#)]
42. Milin, E.; Benaicha, B.; El Hajj, F.; Patinec, V.; Triki, S.; Marchivie, M.; Gómez-García, C.J.; Pillet, S. Magnetic Bistability in Macrocycle-Based Fe^{II} Spin-Crossover Complexes: Counter Ion and Solvent Effects. *Eur. J. Inorg. Chem.* **2016**, *34*, 5305–5314. [[CrossRef](#)]
43. Drahoš, B.; Trávníček, Z. Spin crossover Fe(II) complexes of a cross-bridged cyclam derivative. *Dalton Trans.* **2018**, *47*, 6134–6145. [[CrossRef](#)] [[PubMed](#)]
44. Vithanarachchi, S.M.; Kovacs, D.; Borbas, K.E. Synthesis and photophysical characterization of luminescent lanthanide complexes of nucleotide-functionalized cyclen- and dipicolinate-based ligands. *Inorg. Chim. Acta* **2017**, *460*, 148–158. [[CrossRef](#)]
45. El Hajj, F.; Patinec, V.; Triki, S.; Handel, H.; Marchivie, M. Isomerism as a remarkable tool for the design of new potentially bridging macrocycle ligands: Synthesis and characterization of the [Cu(4-L1)](NO₃)₂·2H₂O polymeric chain (4-L1=mono-*N* (4-picoly) cyclen). *Inorg. Chem. Commun.* **2010**, *13*, 1314–1316. [[CrossRef](#)]
46. Batsanov, A.S.; Goeta, A.E.; Howard, J.A.K.; Maffeo, D.; Puschmann, H.; Williams, J.A.G. Nickel(II) complexes of the isomeric tetraazamacrocyclic ligands 1,11- and 1,8-bis(2-pyridylmethyl)-cyclam and of a structurally constrained *N*⁴,*N*⁸-methylene bridged analogue. *Polyhedron* **2001**, *20*, 981–986. [[CrossRef](#)]
47. Comba, P.; Luther, S.M.; Maas, O.; Pritzkow, H.; Vielfort, A. Template Synthesis of a Tetraazamacrocyclic Ligand with Two Pendant Pyridinyl Groups: Properties of the Isomers of the Metal-Free Ligand and of Their First-Row Transition Metal Compounds. *Inorg. Chem.* **2001**, *40*, 2335–2345. [[CrossRef](#)] [[PubMed](#)]
48. Bu, X.-H.; Lu, S.-L.; Zhang, R.-H.; Liu, H.; Zhu, H.-P.; Liu, Q.-T. Synthesis, characterization and crystal structures of the cobalt(II) and iron(II) complexes with an octadentate ligand, 1,4,7,10-tetrakis(2-pyridylmethyl)-1,4,7,10-tetraazacyclododecane (L), [ML]²⁺. *Polyhedron* **2000**, *19*, 431–435.
49. Bu, X.-H.; Chen, W.; Mu, L.-J.; Zhang, Z.-H.; Zhang, R.-H.; Clifford, T. Syntheses, crystal structures and properties of new manganese(II) complexes with macrocyclic polyamine ligands bearing pyridyl donor pendants. *Polyhedron* **2000**, *19*, 2095–2100. [[CrossRef](#)]
50. Christiansen, L.; Hendrickson, D.N.; Toftlund, H.; Wilson, S.R.; Xie, C.L. Synthesis and structure of metal complexes of triaza macrocycles with three pendant pyridylmethyl arms. *Inorg. Chem.* **1986**, *25*, 2813–2818. [[CrossRef](#)]
51. Shepherd, A.J.; Rosa, P.; Fallis, I.A.; Guionneau, P.; Howard, J.A.K.; Goeta, A.E. Structural origin of the gradual spin transition in a mononuclear iron(II) complex. *J. Phys. Chem. Solids* **2012**, *73*, 193–197. [[CrossRef](#)]

52. Al-Obaidi, A.H.R.; McGarvey, J.J.; Taylor, K.P.; Bell, S.E.J.; Jensen, K.B.; Toftlund, H. Observation of biphasic kinetics in light-induced spin-state crossover in an iron(II) complex in solution. *J. Chem. Soc. Chem. Commun.* **1993**, *6*, 536–538. [[CrossRef](#)]
53. Touti, F.; Maurin, P.; Canaple, L.; Beuf, O.; Hasserodt, J. Awakening of a Ferrous Complex's Electronic Spin in an Aqueous Solution Induced by a Chemical Stimulus. *Inorg. Chem.* **2012**, *51*, 31–33. [[CrossRef](#)] [[PubMed](#)]
54. McGowan, P.C.; Temple, C.N. New N-monofunctionalised 1,4,7-triazacyclononane complexes of iron. *Inorg. Chim. Acta* **2009**, *362*, 3165–3171. [[CrossRef](#)]
55. Stavila, V.; Allali, M.; Canaple, L.; Stortz, Y.; Franc, C.; Maurin, P.; Beuf, O.; Dufay, O.; Samarut, J.; Janier, M.; et al. Significant relaxivity gap between a low-spin and a high-spin iron(II) complex of structural similarity: An attractive off-on system for the potential design of responsive MRI probes. *New J. Chem.* **2008**, *32*, 428–435. [[CrossRef](#)]
56. Gott, A.L.; McGowan, P.C.; Podesta, T.J.; Thornton-Pett, M. Pendant arm N-monofunctionalised 1,4,7-triazacyclononane complexes of Fe(II) and Ru(II). *J. Chem. Soc. Dalton Trans.* **2002**, *18*, 3619–3623. [[CrossRef](#)]
57. Fallis, I.A.; Farley, R.D.; Abdul Malik, K.M.; Murphy, D.M.; Smith, H.J. Divalent first-row transition metal complexes of the rigid pendant-arm ligand 1,4,7-tris(2-aminophenyl)-1,4,7-triazacyclononane. *J. Chem. Soc. Dalton Trans.* **2000**, *20*, 3632–3639. [[CrossRef](#)]
58. Spiccia, L.; Fallon, G.D.; Grannas, M.J.; Nichols, P.J.; Tiekink, E.R.T. Synthesis and characterization of mononuclear and binuclear iron(II) complexes of pentadentate and bis(pentadentate) ligands derived from 1,4,7-triazacyclononane. *Inorg. Chim. Acta* **1998**, *279*, 192–199. [[CrossRef](#)]
59. de Martino Norante, G.; Di Vaira, M.; Mani, F.; Mazzi, S.; Stoppioni, P. Transition metal complexes of a functionalised triazamacrocycle. *J. Chem. Soc. Dalton Trans.* **1992**, *3*, 361–365. [[CrossRef](#)]
60. Guillou, A.; Lima, L.M.P.; Roger, M.; Esteban-Gómez, D.; Delgado, R.; Platas-Iglesias, C.; Patinec, V.; Tripier, R. 1,4,7-Triazacyclononane-Based Bifunctional Picolinate Ligands for Efficient Copper Complexation. *Eur. J. Inorg. Chem.* **2017**, *2017*, 2435–2443. [[CrossRef](#)]
61. Roger, A.; Lima, L.M.P.; Frindel, M.; Platas-Iglesias, C.; Gestin, J.F.; Delgado, R.; Patinec, V.; Tripier, R. Monopicolinate-dipicolyl Derivative of Triazacyclononane for Stable Complexation of Cu²⁺ and ⁶⁴Cu²⁺. *Inorg. Chem.* **2013**, *52*, 5246–5259. [[CrossRef](#)] [[PubMed](#)]
62. Gasser, G.; Tjioe, L.; Graham, B.; Belousoff, M.J.; Juran, S.; Walther, M.; Künstler, J.U.; Bergmann, R.; Stephan, H.; Spiccia, L. Synthesis, Copper(II) Complexation, ⁶⁴Cu-Labeling, and Bioconjugation of a New Bis(2-pyridylmethyl) Derivative of 1,4,7-Triazacyclononane. *Bioconjugate Chem.* **2008**, *19*, 719–730. [[CrossRef](#)] [[PubMed](#)]
63. Arends, I.W.C.E.; Gamez, P.; Sheldon, R.A. Green oxidation of alcohols using biomimetic Cu complexes and Cu enzymes as catalysts. *Adv. Inorg. Chem.* **2006**, *58*, 235–279.
64. Belle, C.; Rammal, W.; Pierre, J.L. Sulfur ligation in copper enzymes and models. *Inorg. Biochem.* **2005**, *99*, 1929–1936. [[CrossRef](#)] [[PubMed](#)]
65. Boulatov, R. Understanding the reaction that powers this world: Biomimetic studies of respiratory O₂ reduction by cytochrome oxidase. *Pure Appl. Chem.* **2004**, *76*, 303–319. [[CrossRef](#)]
66. Himes, R.A.; Karlin, K.D. Copper–dioxygen complex mediated C–H bond oxygenation: Relevance for particulate methane monooxygenase (pMMO). *Curr. Opin. Chem. Biol.* **2009**, *13*, 119–131. [[CrossRef](#)] [[PubMed](#)]
67. Wadas, T.J.; Wong, E.H.; Weisman, G.R.; Anderson, C.J. Coordinating Radiometals of Copper, Gallium, Indium, Yttrium, and Zirconium for PET and SPECT Imaging of Disease. *Chem. Rev.* **2010**, *110*, 2858–2902. [[CrossRef](#)] [[PubMed](#)]
68. Price, E.W.; Orvig, C. Matching chelators to radiometals for radiopharmaceuticals. *Chem. Soc. Rev.* **2014**, *43*, 260–290. [[CrossRef](#)] [[PubMed](#)]
69. Tseberlidis, G.; Intrieri, D.; Caselli, A. Catalytic Applications of Pyridine-Containing Macrocyclic Complexes. *Eur. J. Inorg. Chem.* **2017**, *30*, 3589–3603. [[CrossRef](#)]
70. Guionneau, P.; Marchivie, M.; Bravic, G.; Létard, J.-F.; Chasseau, D. Structural Aspects of Spin Crossover. Example of the [Fe^{II}L_n(NCS)₂] Complexes. *Top. Curr. Chem.* **2004**, *234*, 97–128.
71. Roger, A.; Patinec, V.; Tripier, R.; Triki, S.; Le Poul, N.; Le Mest, Y. Synthesis of an unsymmetrical N-functionalized triazacyclononane ligand and its Cu(II) complex. *Inorg. Chim. Acta* **2014**, *417*, 201–207. [[CrossRef](#)]

72. Farrugia, L.J. ORTEP-3 for Windows—A version of ORTEP-III with a Graphical User Interface (GUI). *J. Appl. Cryst.* **1997**, *30*, 565. [[CrossRef](#)]
73. Oxford Diffraction. *Xcalibur CCD/RED CrysAlis Software System*; Oxford-Diffraction Ltd.: Abingdon, UK, 2006.
74. Sheldrick, A. SHELX97. In *Program for Crystal Structure Analysis*; University of Gottingen: Gottingen, Germany, 1997.
75. Dolomanov, O.V.; Bourhis, L.J.; Gildea, R.J.; Howard, J.A.K.; Puschmann, H. OLEX2: A complete structure, refinement and analysis program. *J. Appl. Crystallogr.* **2009**, *42*, 339–341. [[CrossRef](#)]



© 2019 by the authors. Licensee MDPI, Basel, Switzerland. This article is an open access article distributed under the terms and conditions of the Creative Commons Attribution (CC BY) license (<http://creativecommons.org/licenses/by/4.0/>).